Article ID: 1000-7032(2023)06-0964-11

LuYAG:Ce Transparent Ceramic Phosphors for High-brightness Solid-state Lighting Application

HUANG Xinyou[1], WANG Yanbin[1,2], CHENG Ziqiu[2,3], CHEN Haohong[2,3], DAI Zhengfa[2], TIAN Feng[2,3], CHEN Penghui[2,3], HU Song[2,3], ZHOU Guohong[2,3], LI Jiang[2,3*]

(1. *School of Material Science and Engineering, Jiangsu University, Zhenjiang* 212013, *China*;
2. *Transparent Ceramics Research Center, Shanghai Institute of Ceramics, Chinese Academy of Sciences, Shanghai* 201899, *China*;
3. *Center of Materials Science and Optoelectronics Engineering, University of Chinese Academy of Sciences, Beijing* 100049, *China*)

* *Corresponding Author, E-mail: lijiang@ mail. sic. ac. cn*

Abstract: Achieving high luminous efficiency, high brightness and good thermal stability is an urgent requirement for solid-state lighting. Therefore, the high-performance color converters for high-power light-emitting diodes or laser diodes (LEDs/LDs) are significant to be explored. In this work, an effective strategy to improve the luminescent properties of YAG:Ce color converters through method of component regulation was realized in YAG:Ce transparent ceramic phosphors (TCPs) by incorporating Lu^{3+} ions. We prepared $(Lu,Y)_3Al_5O_{12}$:Ce TCPs (LuYAG:Ce TCPs) with different Lu^{3+} contents by the solid-state reaction and vacuum sintering method. With the increase of Lu^{3+} content, the Y^{3+} sites in LuYAG:Ce TCPs were substituted by Lu^{3+} sites, and the emission peaks of Ce^{3+} were blue-shifted from 573 nm to 563 nm. When the Lu^{3+} content was 60%, the emission intensity reached the maximum value and the luminous efficiency reached 114 $lm \cdot W^{-1}$ by combining the LuYAG:Ce TCPs with a blue LED. A 450 nm laser source was used to construct a laser-driven lighting device in a transmission mode. As the power density increased from 2.2 $W \cdot mm^{-2}$ to 39 $W \cdot mm^{-2}$, the luminous flux of the TCP with 60% Lu^{3+} substitution increased from 128 lm to 1 874 lm with no signs of luminescence saturation and the optimum luminous efficiency reached 128 $lm \cdot W^{-1}$. Thus, the LuYAG:Ce TCPs are expected to be potential color conversion materials for high-power LEDs/LDs lighting.

Key words: $(Lu,Y)_3Al_5O_{12}$:Ce transparent ceramic phosphors (TCPs); solid-state lighting; color conversion materials; high-brightness

CLC number: O482.31 **Document code**: A **DOI**: 10.37188/CJL.20220435

高亮度固态照明用LuYAG:Ce荧光陶瓷

黄新友[1], 王雁斌[1,2], 程梓秋[2,3], 陈昊鸿[2,3], 代正发[2], 田 丰[2,3], 陈鹏辉[2,3], 胡 松[2,3], 周国红[2,3], 李 江[2,3*]

(1. 江苏大学 材料科学与工程学院, 江苏 镇江 212013; 2. 中国科学院上海硅酸盐究所 透明陶瓷研究中心, 上海 201899;
3. 中国科学院大学 材料科学与光电工程中心, 北京 100049)

摘要: 实现高发光效率、高亮度和良好的热稳定性是固态照明的迫切要求。因此,用于高功率发光二极管或激光二极管(LED/LD)的高性能荧光转换材料具有重要的研究意义。在这项工作中, 通过将Lu^{3+}离子引入YAG:Ce荧光陶瓷中方法作为有效策略来改善YAG:Ce荧光材料的发光性能。采用固相反应和真空烧结法制

收稿日期: 2022-12-31; **修订日期**: 2023-01-30
基金项目: 中国科学院战略性先导科技专项(XDA22010301)
Supported by The Strategic Priority Research Program of The Chinese Academy of Sciences (XDA22010301)

备了不同Lu^{3+}含量的$(Lu,Y)_3Al_5O_{12}$:Ce荧光陶瓷(LuYAG:Ce荧光陶瓷)。随着Lu^{3+}含量的增加,LuYAG:Ce荧光陶瓷中的Y^{3+}位点被Lu^{3+}位点取代,Ce^{3+}的发射峰呈现从573 nm到563 nm的蓝移现象。当Lu^{3+}含量为60%时,通过将LuYAG:Ce荧光陶瓷与蓝光LED组合,其发光强度达到最大值,流明效率达到114 $lm\cdot W^{-1}$。使用450 nm激光源与LuYAG:Ce荧光陶瓷构建了透射模式下的激光驱动照明装置。随着功率密度从2.2 $W\cdot mm^{-2}$增加到39 $W\cdot mm^{-2}$,Lu^{3+}含量为60%的荧光陶瓷光通量从128 lm增加到1 874 lm,且没有发光饱和的迹象,最佳发光效率达到128 $lm\cdot W^{-1}$。因此,LuYAG:Ce荧光陶瓷有望成为高功率LED/LD照明的潜在荧光转换材料。

关　键　词:$(Lu,Y)_3Al_5O_{12}$:Ce荧光陶瓷; 固态照明; 荧光转换材料; 高亮度

1　Introduction

Solid-state lighting (SSL) owns the advantages of high brightness, high efficiency, long service life and environmental protection, which has been widely used in automobile, aviation and navigation, *etc*[1-5]. Commonly used solid-state illuminators are mainly composed of color conversion materials and blue light-emitting diodes (LEDs). Color conversion materials mainly include phosphor, phosphor in glasses (PiGs), single crystal phosphors (SCPs) and transparent ceramic phosphors (TCPs)[6-7]. With the development of high-brightness and high-efficiency laser diodes (LDs), thermally quenchable phosphor and PiGs are gradually substituted by SCPs and TCPs with better thermal stability[8-11]. Transparent ceramic phosphors possess good thermal properties and high chemical stability, as well as the advantages of adjustable microstructure and simple preparation process, which is lower cost than SCPs[11-13]. The widely used yellow phosphor $Y_3Al_5O_{12}:Ce^{3+}$ (YAG:Ce) TCPs can be excited to yellow light by blue light, and then the yellow light can mixed with the transmitted blue light to generate white light[14-17]. Component regulation of YAG:Ce phosphor has been proven to be a reliable strategy to improve the luminescence performance of TCPs. For instance, introducing Gd^{3+}, Mg^{2+}-Si^{4+} pairs, Sc^{3+} and Lu^{3+}-Sc^{3+} pairs into YAG:Ce phosphor can effectively regulate spectral characteristics and improve luminescent properties[18-23]. However, the increasing power density of blue LEDs and LDs put forward higher requirements on the thermal stability of YAG:Ce TCPs. Therefore, it is significant to obtain the YAG:Ce TCPs with excellent thermal stability.

$Lu_3Al_5O_{12}:Ce^{3+}$(LuAG:Ce) TCPs are also suitable for high-power SSLs, which have many advantages such as high luminous efficiency and low thermal quenching among common phosphors, but LuAG:Ce TCPs require stricter sintering condition[24-27]. Lu^{3+} (175) ions have a higher atomic weight than Y^{3+} (89) ions and the 4f sublayer of Lu^{3+} ions is completely filled with electrons, leading to the thermal stability of LuAG higher than that of YAG[28-34]. Therefore, replacing Y^{3+} sites with Lu^{3+} sites in YAG:Ce TCPs can not only improve the thermal stability but also maintain excellent luminescent properties. At present, there are some researches about LuYAG:Ce TCPs. For example, Ling *et al.* [35] prepared a series of LuYAG:Ce TCPs and obtained exclent LED luminous properties. However, there are still few relevant studies about LuYAG:Ce TCPs and luminescent properties for LD lighting need to be further explored. In this work, we investigated the variation of crystal structure and spectral characteristics of Ce^{3+} when Lu^{3+} substituted Y^{3+} into the dodecahedron site of the YAG host, which could influence luminescent properties of LuYAG:Ce TCPs, and proved that LuYAG:Ce TCPs have great potential as the color converter for high-brightness SSL applications. A series of LuYAG:Ce TCPs with different Lu^{3+} contents were fabricated by solid-state reactive sintering in vacuum. The phase and microstructure of the ceramics were characterized by XRD and SEM. The in-line transmittance and PL/PLE spectra were tested. The luminous properties such as luminous flux and luminous efficiency by combining the prepared ceramics with a high-power blue LED and LD were measured. Moreover, the suitability of LuYAG:Ce TCPs used as color converters for high-brightness solid-state lighting application was evaluated.

2 Experiment

Ceramic samples with the chemical formula of $(Ce_{0.001}Y_{0.999-x}Lu_x)_3Al_5O_{12}$ (x= 0, 0.2, 0.4, 0.6, 0.8, 0.999) were prepared by high temperature solid-state reaction method. Commercial Y_2O_3 (99.999%, Shanghai Sinian metal materials Co., Ltd), Lu_2O_3(99.999%, Jining Zhongkai New Materials Co., Ltd), α-Al_2O_3(99.99%, Fenghe Ceramic Co., Ltd), CeO_2(99.995%, Fujian Changting Golden Dragon Co., Ltd) were used as raw materials. Above raw powders were weighed according to the stoichiometric ratio and then mixed by ball milling for 12 h in ethanol, with 0.8% TEOS(99.999%, Alfa Aesar) and 0.08% MgO(99.998%, Alfa Aesar) as sintering aids. The powder mixtures were dried at 70 ℃ for 2 h, sieved through a 200-mesh screen and calcined at 600 ℃ in air for 4 h to remove the organic impurities. Then mixed powders were pressed into disks with a diameter of 20 mm under 20 MPa and cold-pressed under 250 MPa for 3 min. The pretreated disks were sintered at 1 800 ℃ in vacuum atmosphere for 10 h and annealed at 1 450 ℃ in air for 10 h. Eventually, both sides of the composite ceramics were polished to 1.6 mm for further measurements.

The X-ray diffraction(XRD) patterns of these ceramics were obtained using an X-ray diffractometer (Ultima IV, Rigaku, Japan), with Cu Kα radiation in the angle range covered from 10° to 80°. The microstructure was characterized by a field-emission scanning electron microscopy(FESEM SU8220, Hitachi, Japan). The distribution of pores and impurities in transparent ceramics were analyzed by a transmission optical microscope(TOM BX51, Olympus, Japan). The in-line transmittance curves of the ceramics over the wavelength range from 200 nm to 800 nm were tested by a UV-VIS spectrophotometer (Cary 5000, Varian Medical System Inc. Palo Alto, USA). The photoluminescence(PL) and photoluminescence excitation(PLE) spectra were tested by using the homemade multi-function combined fluorescence spectrum test system (SicOmni-I) equipped with VX-XBO 150 W xenon lamp, Omni-λ3007(Zolix, China) monochromator, PMTH-S1-CR131 photomultiplier tube and LHM254 mercury lamp. These transparent ceramic phosphors were packaged into LED chip-on board(COB) modules with commercial 460 nm blue chips and constructed by a 450 nm laser source in a reflection mode. The related room-temperature luminous efficiency(LE), luminous flux (LF) and electroluminescent properties were measured by an integrating sphere connected to a CCD spectrometer(OHSP-350, Hopoocolor, China).

3 Results and Discussion

Fig. 1 shows FESEM morphologies of the raw powder. The average primary particle size of Y_2O_3 and Lu_2O_3 was 92.1 nm and 241.6 nm respectively by the mathematical statistics method. Moreover, the average primary particle size of α-Al_2O_3 and CeO_2 was calculated to be 177.7 nm and 43.4 nm through conversion of specific surface area. In terms of powder morphology, Y_2O_3 was lamellar and Lu_2O_3

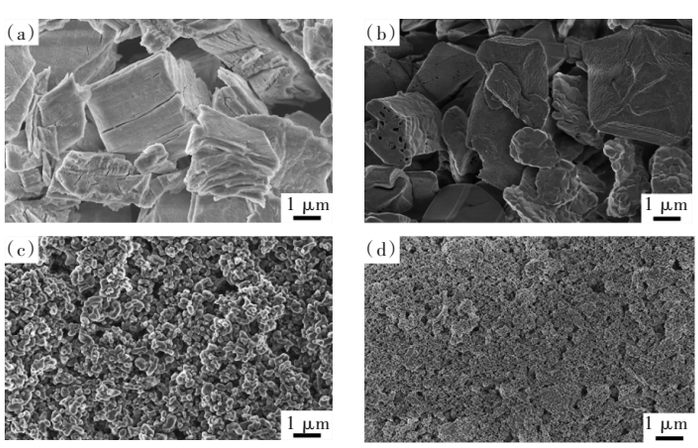

Fig.1 FESEM morphologies of raw material powder. (a)Y_2O_3. (b)Lu_2O_3. (c)α-Al_2O_3. (d)CeO_2.

exhibited massive morphology with mesoporous. Al_2O_3 raw powder presented dumbbell shape with some degree of agglomeration and CeO_2 nano powder was fine and evenly distributed.

Fig. 2 shows LuYAG:Ce TCPs with different Lu^{3+} contents ranging from 0%–99.9%. The double-surface polished ceramics had the diameter of 15 mm and the thickness of 1.6 mm. The text at the bottom of the samples was clearly visible, which indicated the ceramics have great optical transmittance. With the increase of Lu^{3+} content in LuYAG:Ce TCPs, the color of the ceramics changed from yellow to yellow-green under natural illumination, which was related to the absorption of Ce^{3+}.

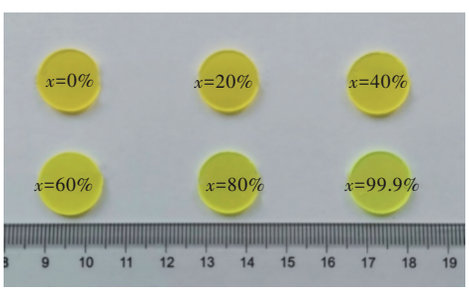

Fig.2　Photograph of 1.6 mm thick LuYAG:Ce TCPs with x%Lu(x= 0, 20, 40, 60, 80, 99.9) under natural illumination

The XRD patterns of the samples are shown in Fig. 3. With the increase of Lu^{3+} content, the characteristic peaks of LuYAG:Ce TCPs conformed to the change from YAG phase(JCPDS#33-0040) to LuAG phase (JCPDS#73-1368), and no hetero peak was detected, indicating that the prepared samples could be a single pure phase or contain a very small amount of unobserved secondary phase. With the addition of CeO_2 into LuYAG, Ce^{4+} would be reduced

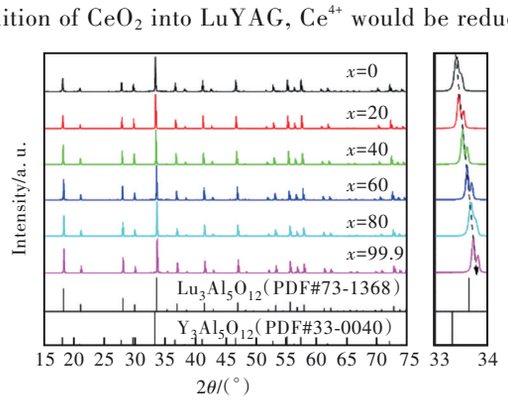

Fig.3　XRD patterns of LuYAG:Ce TCPs with x%Lu(x= 0, 20, 40, 60, 80, 99.9)

to Ce^{3+} under the vacuum sintering condition and enter the lattice to replace the Y^{3+} or Lu^{3+} in the dodecahedron. The 2θ diffraction peaks moved to higher angle between 33° and 34° because the radius of Lu^{3+} (0.084 nm) is slightly smaller than that of Y^{3+} (0.090 nm), which can result in the lattice contraction.

SEM images were carried out to insight the microstructure of LuYAG:Ce TCPs, which were thermally etched at 1 450 ℃ for 3 h in air before SEM observation, as displayed in Fig. 4(a)–(f). It could be found that all the ceramics exhibited clear grain boundaries and some residual visible pores have been detected. Average grain sizes of $(Ce_{0.001}Y_{0.999-x}Lu_x)_3Al_5O_{12}$ TCPs (x = 0, 0.2, 0.4, 0.6, 0.8, 0.999) were measured to be 10.32, 11.73, 20.20, 19.77, 18.31, 25.01 μm, respectively. There was the secondary phase observed from YAG:Ce TCPs. According to the EDS analysis shown in Fig. 5, the part 1 proportion of metal cation Y:Al was 1.6:5, which deviated from normal proportion Y:Al=3:5, so the secondary phase was Al-rich phase, which was most likely Al_2O_3 phase. The secondary phase in YAG:Ce TCP had a few content because it was not observed by XRD patterns of LuYAG:Ce TCPs. As shown in Fig. 4(g)–(l), there were pores observed inside the TCPs, which can reduce the optical quality of the ceramics. Furthermore, it is obvious that more and larger pores can be found inside the $(Lu_{0.6}Y_{0.4})$AG:Ce TCPs, which may be attributed to the more complicated diffusion reaction[36].

The in-line transmittance of LuYAG:Ce TCPs with a thickness of 1.6 mm is shown in Fig. 6(a). The absorption between 300–400 nm and another between 400–500 nm were caused by the $4f^1 \rightarrow 5d^1$ transition of Ce^{3+}. As shown in Fig. 6(b), the in-line transmittance at 800 nm and 400 nm presented a trend of decreasing first and then increasing. When the Lu^{3+} content reached 60%, the in-line transmittance curves of LuYAG:Ce TCPs at 800 nm decreased significantly, which can be caused by the scattering centers in TCPs like pores and the secondary phase.

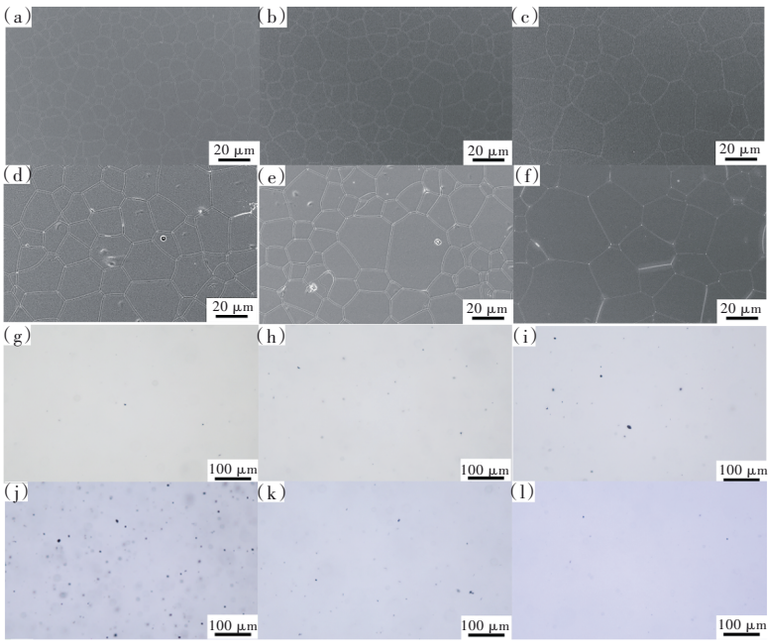

Fig.4 SEM images((a)-(f)) and TOM images((g)-(l)) of the $(Ce_{0.001}Y_{0.999-x}Lu_x)_3Al_5O_{12}$ TCPs(x= 0, 0.2, 0.4, 0.6, 0.8, 0.999)

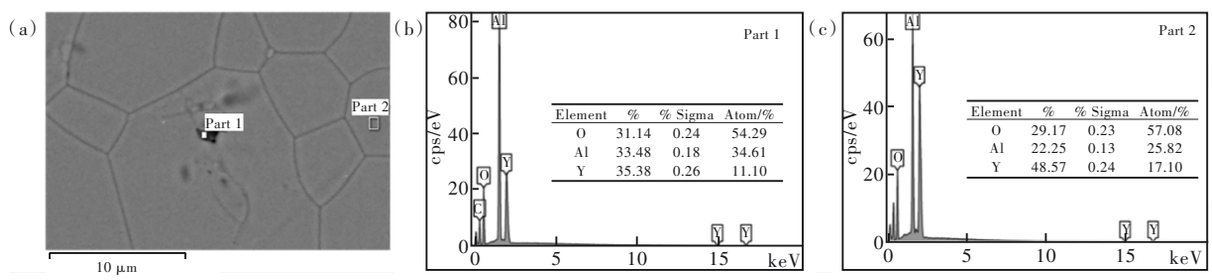

Fig.5 EDS analysis of YAG∶Ce TCP. (a)The select area. (b)The secondary phase. (c)The basal body.

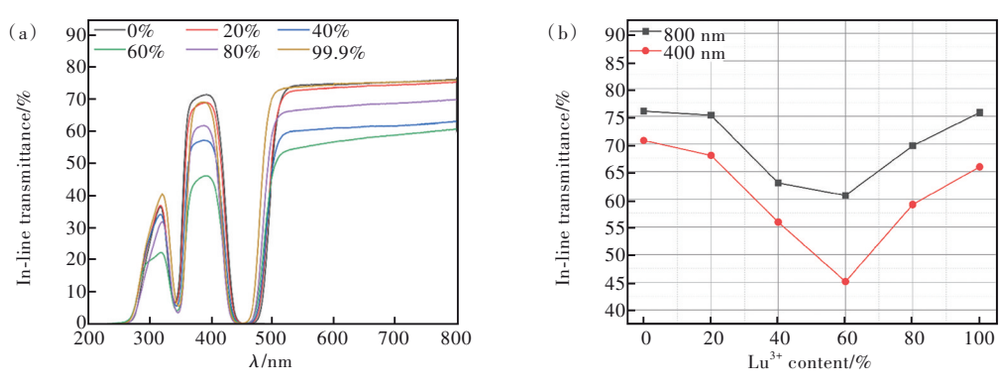

Fig.6 In-line transmittance curves(a) and in-line transmittance(b) at 400 nm and 800 nm of LuYAG∶Ce TCPs with different Lu^{3+} contents

Fig. 7(a) shows the excitation and emission spectra of LuYAG∶Ce TCPs at room temperature. The excitation peaks located between 300-400 nm and 400-500 nm can be attributed to the transition of Ce^{3+} from the ground state $^2F_{5/2}$ to the two excited states $5d_2$ and $5d_1$ respectively, which was consistent with the relevant report[37]. Under the excitation at the wavelength of 469 nm, the emission bands of LuYAG∶Ce TCPs in the range of 500-650 nm originated from the $4f^05d^1 \rightarrow 4f^15d^0$ transition of Ce^{3+}. The 4f orbital was split into two energy levels ($^2F_{5/2}$ and $^2F_{7/2}$) due to spin-orbit coupling. With the increase of Lu^{3+} content, the intensity of excitation and emission peaks presented a trend of first increase and

then decrease. When the Lu^{3+} content was 60%, the intensity of excitation and emission peaks reached the maximum. The reason for this result was related to the in-line transmittance. PLE/PL data collected the reflected light from ceramic surface and the part of internal scattered and refracted light. Thus, the PLE/PL intensity would be lower as TCPs with high in-line transmittance passed through more light.

Fig. 7(b) is the normalized emission spectrum of LuYAG:Ce TCPs. With the increase of Lu^{3+} content, the emission peak position of Ce^{3+} was blue-shifted from 573 nm to 563 nm. This was mainly caused by the following two factors[30,38-40]: on the one hand, the electronegativity of Lu^{3+} (1.27) is greater than that of Y^{3+} (1.22), so the 5d level of Ce^{3+} in LuYAG:Ce TCPs shifts to higher energy level due to the increase of average electronegativity. On the other hand, the radius of Lu^{3+} is smaller than that of Y^{3+}, making the crystal structure of LuYAG:Ce contracted, thereby reducing the degree of splitting of the Ce^{3+} crystal field. Thus, the excitation peak position of Ce^{3+} in normalized PLE spectra ranging 440–480 nm(Fig. 7(c)) was also blue-shifted from 469 nm to 466 nm and the excitation peak position of Ce^{3+} in normalized PLE spectra ranging 320–360 nm(Fig. 7(d)) was red-shifted from 343 nm to 350 nm. Fig. 8 showed the energy levels of the ground state 4f and excited state 5d orbitals of Ce^{3+} in YAG:Ce and LuYAG:Ce. Therefore, the variation in emission and excitation spectra of Ce^{3+} can be attributed to the combined action of above factors.

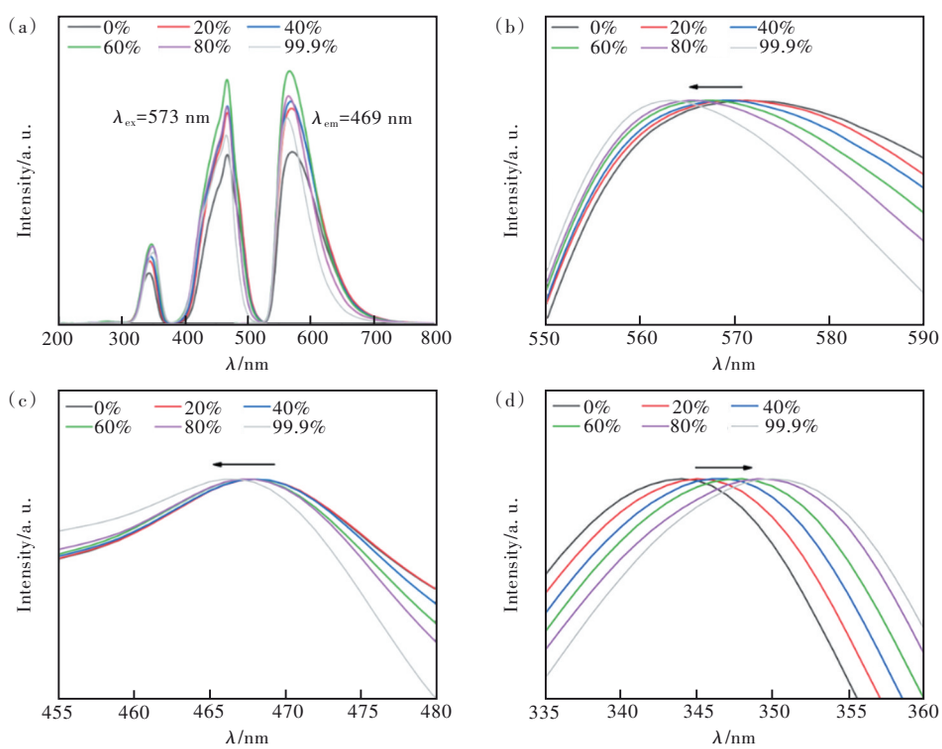

Fig.7 (a)PL and PLE spectra. (b)Normalized PL spectra ranging 550–590 nm. (c)–(d)Normalized PLE spectra ranging 440–480 nm and 320–360 nm of LuYAG:Ce TCPs with different Lu^{3+} contents.

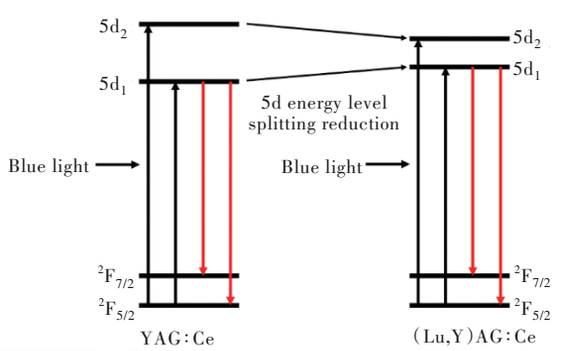

Fig.8 Energy levels diagram of 4f ground state and 5d excited state of Ce^{3+} in YAG:Ce and LuYAG:Ce

Different test methods would obtain different luminescent properties, so LuYAG:Ce TCPs with different Lu^{3+} contents were tested for luminescent properties in a 460 nm LED COB module and a 450 nm LD remote excitation mode respectively to ensure

the reliability of the test results. Fig. 9(a) showed the luminous efficiency and luminous flux of LuYAG:Ce TCPs rose first and then descended under the excitation of 460 nm blue light based on 2.7 W LED devices with the increase of Lu^{3+} content. The reason behind the above phenomenon was that the pores and secondary phases in the ceramics can be scattering centers to increase the optical path of blue light, leading to the enhancement of luminous efficiency[41-42]. According to the TOM images(Fig. 4(g)-(l)), the porosity in LuYAG:Ce TCPs increased first and then decreased with the increase of Lu^{3+}, which was the main reason for the change of luminous efficiency and luminous flux. As the Lu^{3+} content was 60%, the LuYAG:Ce TCP with the maximum content of pores exhibited the optimum luminous efficiency and luminous flux of 114 lm·W^{-1} and 307 lm, respectively, which was verified by the PLE/PL intensity. As shown in Fig. 9(b), the electroluminescent (EL) spectra revealed the exceptionally low peak of 460 nm and the wide band ranging from 475 nm to 750 nm. The extremely low peak of 460 nm indicated the sufficient absorption of the pumping blue light by Ce^{3+}. With the increase of Lu^{3+} content, the broad band ranging from 475 nm to 750 nm rendered more green spectral component, which was related to the spectral blue shift of LuYAG:Ce TCPs, accordingly leading to the correlated color temperature(CCT) ascended from 4 466 to 6 170 and the *Ra* decreased from 38 to 26(Fig. 9(c)). As a result, the chromaticity coordinate also varied from (0.399 3, 0.561 9) to (0.296 8, 0.568)(Fig. 9(d)). Here we compared the results with the study on GdYAG:Ce TCPs applied in LED(luminous efficiency: 63.70-81.75 lm/W)[7]. The luminous efficiency was improved in LuYAG:Ce TCPs used in LED COB module.

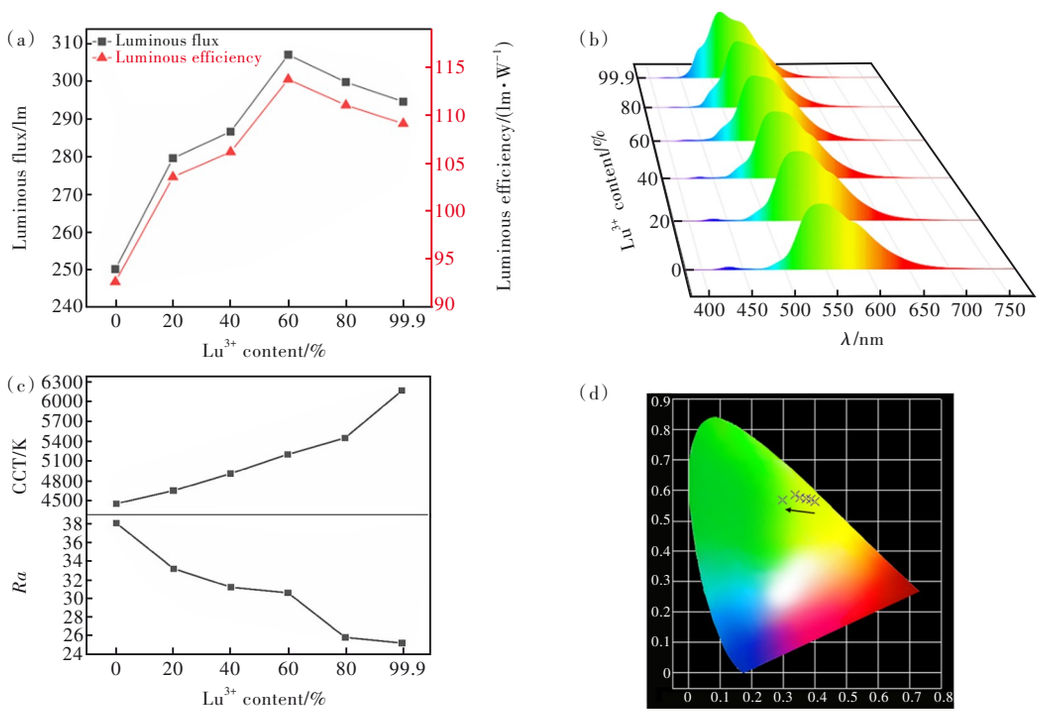

Fig.9 (a) Luminous efficiency and luminous flux. (b) EL spectra. (c) CCT and *Ra*. (d) Chromaticity coordinate of LuYAG:Ce TCPs with different Lu^{3+} contents under blue LED excitation.

The LuYAG:Ce TCPs were constructed by using a 450 nm LD remote excitation in transmission mode (diameter of laser light spot: 0.76 mm). The luminous efficiency, luminous flux and EL spectra at different power densities based laser lighting device were exhibited in Fig. 10. It could be seen that the luminous efficiency and luminous flux of LuYAG:Ce TCPs based LDs showed the similar change trend with those observed from the LED devices. The luminous efficiency and luminous flux of the LD devices (under 2.2 W·mm^{-2} blue laser excitation) reached as high as 128 lm·W^{-1} and 128

lm, respectively (Fig. 10(a)), as the Lu^{3+} content was 60%. By increasing the power density to 27.3 $W \cdot mm^{-2}$, the $(Lu_{0.6}Y_{0.4})AG:Ce$ TCPs acted out superior luminous flux (1 459 lm) than LD devices with the low output power, but the luminous efficiency decreased to 118 $lm \cdot W^{-1}$, which indicated the conversion efficiency from excitation to emission decreased to some extent (Fig. 10(b)). The EL spectra under the excitation of 27.3 $W \cdot mm^{-2}$ LD was shown in Fig. 10(c). Similarly, the wide band ranging from 475 nm to 750 nm rendered more green spectral component with increasing Lu^{3+} content. However, compared with the LED devices, there were more blue components in the EL spectra based LDs, which indicated the part of blue light from LD source was mixed with the conversion ranging from 475 nm to 750 nm rather than absorbed by Ce^{3+}. Fig. 10(d) showed the variety of $(Ce_{0.001}Y_{0.999-x}Lu_x)_3Al_5O_{12}$ TCPs'(x =0.4, 0.6, 0.999) luminous flux with increasing the input power density from 2.2 $W \cdot mm^{-2}$ to 39 $W \cdot mm^{-2}$. As the input power density reached 34 $W \cdot mm^{-2}$, the luminous flux of $(Lu_{0.4}Y_{0.6})AG:Ce$ TCPs reached the optimum and then declined with the further increase of power density. However, $(Lu_{0.6}Y_{0.4})AG:Ce$ TCPs exhibited no luminescence saturation with the power density increased to 39 $W \cdot mm^{-2}$ (Maximum power density of equipment), and presented the optimum luminous flux of 1 874 lm, which was higher than LuAG:Ce TCPs (1 850 lm). Therefore, LuYAG:Ce TCPs are promising color converters for use in high-brightness SSL applications.

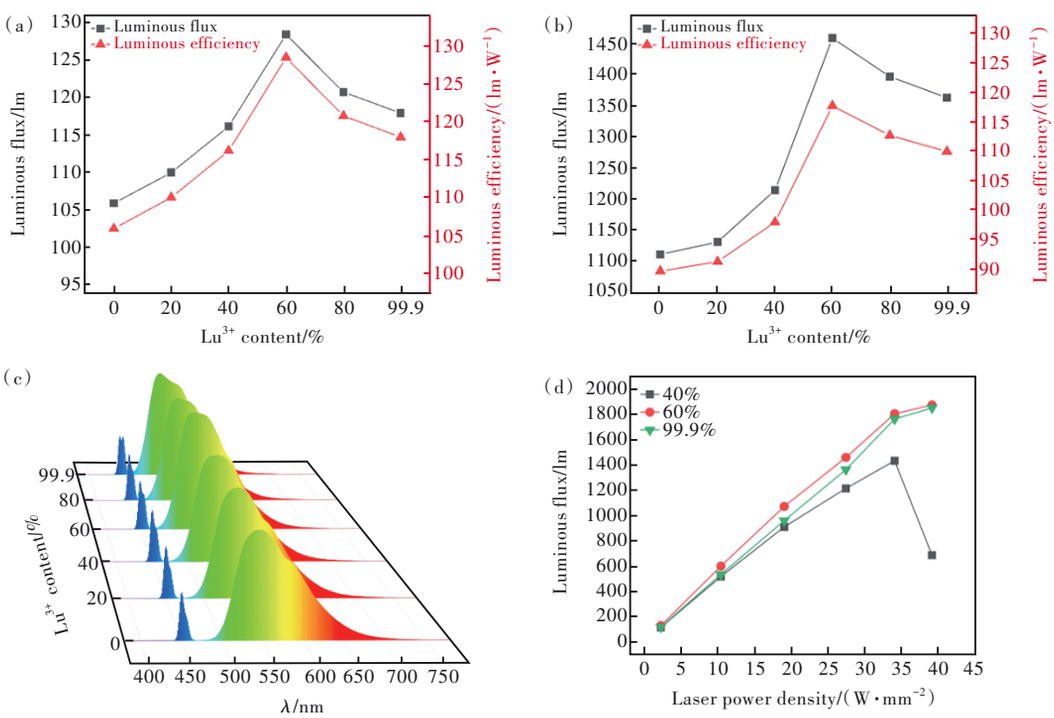

Fig.10　Luminous efficiency and luminous flux of LuYAG:Ce TCPs with different Lu^{3+} contents under 2.2 $W \cdot mm^{-2}$(a) and 27.3 $W \cdot mm^{-2}$(b) blue laser excitation. (c)EL spectra under 27.3 $W \cdot mm^{-2}$ blue laser excitation. (d)Luminous flux as a function of laser power density.

4　Conclusion

In summary, a series of LuYAG:Ce TCPs with different Lu^{3+} contents were prepared by the solid-state reaction method. The microstructure and optical properties of LuYAG:Ce TCPs were investigated. It turned out that Lu^{3+} sites can successfully enter the YAG lattice and replace Y^{3+} sites to form LuYAG:Ce phase, which could improve the thermal stability of LuYAG:Ce TCPs to ensure high brightness and efficiency in lighting applications. The $(Lu_{0.6}Y_{0.4})AG:Ce$ TCPs exhibited a high luminous efficiency of 114 $lm \cdot W^{-1}$ by combining the LuYAG:Ce TCs with a 460 nm blue LED chip and demonstrated

the optimum luminous efficiency of 128 $lm \cdot W^{-1}$ and luminous flux of 128-1 874 lm under the excitation of different incident laser power densities (2.2-39 $W \cdot mm^{-2}$). Therefore, the results indicate that the designed TCPs can be prospectively potential in phosphor converters for high-brightness SSL applications.

Response Letter is available for this paper at: http://cjl.lightpublishing.cn/thesisDetails#10.37188/CJL.20220435.

References:

[1] CI H N, CHANG H L, WANG R Y, *et al*. Enhancement of heat dissipation in ultraviolet light-emitting diodes by a vertically oriented graphene nanowall buffer layer [J]. *Adv. Mater.*, 2019, 31(29): 1901624-1-8.

[2] LING J R, ZHOU Y F, XU W T, *et al*. Red-emitting YAG:Ce, Mn transparent ceramics for warm WLEDs application [J]. *J. Adv. Ceram.*, 2020, 9(1): 45-54.

[3] TANG Y, LIU B, YAN N, *et al*. Perovskite quantum dot-coated YAG:Ce composites for warm white light-emitting diodes [J]. *Opt. Mater.*, 2022, 127: 112309-1-9.

[4] 彭星淋, 李淑星, 刘泽华, 等. 大功率固态照明用荧光陶瓷研究进展 [J]. 无机材料学报, 2021, 36(8): 807-819.
PENG X L, LI S X, LIU Z H, *et al*. Phosphor ceramics for high-power solid-state lighting [J]. *J. Inorg. Mater.*, 2021, 36(8): 807-819. (in Chinese)

[5] PUST P, SCHMIDT P J, SCHNICK W. A revolution in lighting [J]. *Nat. Mater.*, 2015, 14(5): 454-458.

[6] ZHANG J F, GU G R, DI X X, *et al*. Optical characteristics of Ce, Eu:YAG single crystal grown by Czochralski method [J]. *J. Rare Earths*, 2019, 37(2): 145-150.

[7] 邵秀晨, 周圣明, 唐燕如, 等. Ce:YAG荧光陶瓷掺杂Gd对白光LED发光性能的影响 [J]. 无机材料学报, 2018, 33(10): 1119-1123.
SHAO X C, ZHOU S M, TANG Y R, *et al*. Luminescence characteristics of Ce:YAG ceramic phosphors with Gd^{3+} doping for white light-emitting diodes [J]. *J. Inorg. Mater.*, 2018, 33(10): 1119-1123. (in Chinese)

[8] XU J, LIU X, LI J. Solid-state lighting [M]. IKESUE A. *Processing of Ceramics: Breakthroughs in Optical Materials. Hoboken: Wiley*, 2021.

[9] ZHANG Y Q, LIU J M, ZHANG Y J, *et al*. Robust YAG:Ce single crystal for ultra-high efficiency laser lighting [J]. *J. Rare Earths*, 2022, 40(5): 717-724.

[10] ZHAO H Y, YU H Q, XU J, *et al*. Novel high-thermal-conductivity composite ceramic phosphors for high-brightness laser-driven lighting [J]. *J. Mater. Chem. C*, 2021, 9(32): 10487-10496.

[11] ZHAO H Y, LI Z, ZHANG M W, *et al*. High-performance Al_2O_3-YAG:Ce composite ceramic phosphors for miniaturization of high-brightness white light-emitting diodes [J]. *Ceram. Int.*, 2020, 46(1): 653-662.

[12] TIAN Y N, CHEN J, YI X Z, *et al*. A new $BaAl_2O_4$-YAG:Ce composite ceramic phosphor for white LEDs and LDs lighting [J]. *J. Eur. Ceram. Soc.*, 2021, 41(7): 4343-4348.

[13] LU H, SONG Q S, XU X D, *et al*. Improving the CRI of Al_2O_3-YAG:Ce eutectic for high-power white LEDs applications: energy-transfer and co-luminescence [J]. *Opt. Mater.*, 2021, 121: 111415.

[14] LIU X, QIAN X L, ZHENG P, *et al*. Composition and structure design of three-layered composite phosphors for high color rendering chip-on-board light-emitting diode devices [J]. *J. Adv. Ceram.*, 2021, 10(4): 729-740.

[15] YAO Q, HU P, SUN P, *et al*. YAG:Ce^{3+} transparent ceramic phosphors brighten the next-generation laser-driven lighting [J]. *Adv. Mater.*, 2020, 32(19): 1907888-1-7.

[16] TIAN Y N, TANG Y R, YI X Z, *et al*. The analyses of structure and luminescence in $(Mg_yY_{3-y})(Al_{5-y}Si_y)O_{12}$ and $Y_3(Mg_xAl_{5-2x}Si_x)O_{12}$ ceramic phosphors [J]. *J. Alloys Compd.*, 2020, 813: 152236-1-8.

[17] JIA J J, QIANG Y C, XU J F, *et al*. A comparison study on the substitution of Y^{3+}-Al^{3+} by M^{2+}-Si^{4+} (M=Ba, Sr, Ca, Mg) in $Y_3Al_5O_{12}$:Ce^{3+} phosphor [J]. *J. Am. Ceram. Soc.*, 2020, 103(9): 5111-5119.

[18] DU A C, DU Q Y, LIU X, *et al*. Ce:YAG transparent ceramics enabling high luminous efficacy for high-power LEDs/LDs [J]. *J. Inorg. Mater.*, 2021, 36(8): 883-892.

[19] ZHENG P, LI S X, WEI R, *et al*. Unique design strategy for laser-driven color converters enabling superhigh-luminance

and high-directionality white light [J]. *Laser Photonics Rev.*, 2019, 13(10): 1900147-1-10.

[20] MA Y L, ZHANG L, ZHOU T Y, *et al.* Weak thermal quenching and tunable luminescence in Ce:$Y_3(Al, Sc)_5O_{12}$ transparent ceramics for high power white LEDs/LDs [J]. *Chem. Eng. J.*, 2020, 398: 125486-1-14.

[21] MA Y L, ZHANG L, HUANG J, *et al.* Broadband emission $Gd_3Sc_2Al_3O_{12}:Ce^{3+}$ transparent ceramics with a high color rendering index for high-power white LEDs/LDs [J]. *Opt. Express*, 2021, 29(6): 9474-9493.

[22] FENG S W, QIN H M, WU G Q, *et al.* Spectrum regulation of YAG:Ce transparent ceramics with Pr, Cr doping for white light emitting diodes application [J]. *J. Eur. Ceram. Soc.*, 2017, 37(10): 3403-3409.

[23] 李江, 李万圆, 刘欣, 等. 固态照明/显示用荧光陶瓷研究进展 [J]. 发光学报, 2021, 42(5): 580-604.
LI J, LI W Y, LIU X, *et al.* Research progress on phosphor ceramics for solid-state lighting/display [J]. *J. Inorg. Mater.*, 2021, 42(5): 580-604. (in Chinese)

[24] 丁慧, 胡盼, 刘永福, 等. LuAG:Ce^{3+}在激光照明应用中的研究进展 [J]. 发光学报, 2021, 42(10): 1531-1548.
DING H, HU P, LIU Y F, *et al.* Recent progress of LuAG:Ce^{3+} for white laser diode lighting application [J]. *Chin. J. Lumin.*, 2021, 42(10): 1531-1548. (in Chinese)

[25] LING J R, ZHANG Y, YANG J, *et al.* A single-structured LuAG:Ce,Mn phosphor ceramics with high CRI for high-power white LEDs [J]. *J. Am. Ceram. Soc.*, 2022, 105(9): 5738-5750.

[26] XU J, WANG J, GONG Y X, *et al.* Investigation of an LuAG:Ce translucent ceramic synthesized *via* spark plasma sintering: towards a facile synthetic route, robust thermal performance, and high-power solid state laser lighting [J]. *J. Eur. Ceram. Soc.*, 2018, 38(1): 343-347.

[27] ZHOU T Y, HOU C, ZHANG L, *et al.* Efficient spectral regulation in Ce:$Lu_3(Al,Cr)_5O_{12}$ and Ce:$Lu_3(Al,Cr)_5O_{12}$/Ce:$Y_3Al_5O_{12}$ transparent ceramics with high color rendering index for high-power white LEDs/LDs [J]. *J. Adv. Ceram.*, 2021, 10(5): 1107-1118.

[28] 刘强, 李万圆, 刘欣, 等. 高亮度固态照明用黄绿光发射Ce:LuAG透明陶瓷 [J]. 发光学报, 2021, 42(10): 1520-1530.
LIU Q, LI W Y, LIU X, *et al.* Green-yellow emission Ce:LuAG transparent ceramics for high-brightness solid-state lighting [J]. *Chin. J. Lumin.*, 2021, 42(10): 1520-1530. (in Chinese)

[29] TANG F, SU Z C, LAO X Z, *et al.* The key roles of 4f-level splitting and vibronic coupling in the high-efficiency luminescence of Ce^{3+} ion in LuAG transparent ceramic phosphors [J]. *J. Lumin.*, 2020, 225: 117360.

[30] 李金生, 孙旭东, 李晓东, 等. 硬脂酸盐熔融法合成(Y, Lu)AG:Ce荧光粉及荧光性能研究 [J]. 无机材料学报, 2015, 30(2): 177-182.
LI J S, SUN X D, LI X D, *et al.* (Y, Lu)AG:Ce phosphors synthesized by stearate melting method and their fluorescence properties [J]. *J. Inorg. Mater.*, 2015, 30(2): 177-182. (in Chinese)

[31] KUMAR S A, SUBALAKSHMI K, KUMAR K A, *et al.* Microstructure, luminescence, and dielectric properties of microwave-sintered Ce:LuAG nano-ceramics [J]. *Ceram. Int.*, 2020, 46(17): 27092-27098.

[32] CHEN L, CHEN X L, LIU F Y, *et al.* Charge deformation and orbital hybridization: intrinsic mechanisms on tunable chromaticity of $Y_3Al_5O_{12}:Ce^{3+}$ luminescence by doping Gd^{3+} for warm white LEDs [J]. *Sci. Rep.*, 2015, 5: 11514-1-17.

[33] XU Y R, LI S X, ZHENG P, *et al.* A search for extra-high brightness laser-driven color converters by investigating thermally-induced luminance saturation [J]. *J. Mater. Chem.* C, 2019, 7(37): 11449-11456.

[34] YANG X F, FANG Z Q, KONG W B, *et al.* Efficient Tm:LuYAG laser resonantly pumped by an Er:LuYAG laser [J]. *Opt. Eng.*, 2022, 61(8): 086106.

[35] LING J R, XU W T, YANG J, *et al.* The effect of Lu^{3+} doping upon YAG:Ce phosphor ceramics for high-power white LEDs [J]. *J. Eur. Ceram. Soc.*, 2021, 41(12): 5967-5976.

[36] FENG Y G, XIE T F, CHEN X P, *et al.* Fabrication, microstructure and optical properties of Yb:$Lu_xY_{3-x}Al_5O_{12}$ transparent ceramics [J]. *Opt. Mater.*, 2020, 110: 110478.

[37] LI D Y, XU W, ZHOU D L, *et al.* Cerium-doped perovskite nanocrystals for extremely high-performance deep-ultraviolet photoelectric detection [J]. *Adv. Opt. Marer.*, 2021, 9(22): 2100423-1-8.

[38] CAO X, SUN S C, LU B, *et al.* Spectral photoluminescence properties of YAG:Ce, *R* (*R*: Gd^{3+}, Pr^{3+}, Gd^{3+} and Pr^{3+}) transparent fluorescent thin film prepared by pulse laser deposition [J]. *J. Lumin.*, 2020, 223: 117222-1-9.

[39] DORENBOS P. Relating the energy of the [Xe]$5d^1$ configuration of Ce^{3+} in inorganic compounds with anion polarizability

and cation electronegativity [J]. *Phys. Rev.* B, 2002, 65(23): 235110-1-1.

[40] SEIJO L, BARANDIARAN Z. Host effects on the optically active 4f and 5d levels of Ce^{3+} in garnets [J]. *Phys. Chem. Chem. Phys.*, 2013, 15(44): 19221-19231.

[41] LIU Z H, LI S X, HUANG Y H, *et al*. Composite ceramic with high saturation input powder in solid-state laser lighting: microstructure, properties, and luminous emittances [J]. *Ceram. Int.*, 2018, 44(16): 20232-20238.

[42] FANG H L, ZHOU B Y, WANG J C, *et al*. Y_2O_3-YAG:Ce composite phosphor ceramics with enhanced light extraction efficiency for solid-state laser lighting [J]. *J. Mater. Chem.* C, 2022, 10(42): 16147-16156.

黄新友(1963-),男,江苏镇江人,博士,教授,硕士生导师,2008年于江苏大学获得博士学位,主要从事发光材料和透明陶瓷等方面的研究。

E-mail: huangxy@ujs.edu.cn

李江(1977-),男,浙江绍兴人,博士,研究员,博士生导师,2007年于中国科学院上海硅酸盐研究所获得博士学位,主要从事光功能透明陶瓷方面的研究。

E-mail: lijiang@mail.sic.ac.cn